JTTEE5 8:57-67

In-Situ Particle Temperature, Velocity, and Size Measurements in DC Arc Plasma Thermal Sprays

B.M. Cetegen and W. Yu

(Submitted 25 June 1998; in revised form 11 September 1998)

Particle temperature, velocity, and size measurements in DC arc plasma thermal sprays are reported in this article. Experiments were performed using a conventional DC arc argon-hydrogen plasma with two 7 wt % yttria-stabilized zirconia powders injected transversely into the plasma jet. Measurements were performed along the axis of the plasma jet as well as at a number of radial locations at several axial positions. It was found that transverse injection of the powder results in the aerodynamic size classification of the powder with the large particles penetrating further across the plasma jet than the smaller particles, which were more readily swept by the high momentum of the plasma jet. Consequently, the particle temperatures were influenced by their degree of penetration into the core of the plasma jet. Average particle temperatures showed a good degree of uniformity radially and decayed with increasing downstream distance. When nanoclustered particles were injected into the plasma, significant differences in particle velocities and temperatures were observed in comparison to the conventional powder under the same plasma operating and particle injection conditions. These differences were attributed to the penetration characteristics of the powder into the plasma jet and the consequent effects on the particle heat up. Hence, axial injection of powder into plasma jets may provide more uniform and axisymmetric particle property distributions compared to the transverse injection schemes.

Keywords DC arc plasmas, in-flight particle temperature, optical diagnostics, particle injection, thermal barrier coatings, velocity and size measurements

1. Introduction

Thermal spray processes are commonly employed to apply metallic and nonmetallic (typically ceramic) coatings in many industrial applications. Examples span applications in the automotive industry for engine part coatings, in aerospace applications such as gas turbine thermal barrier coatings, in the machine tool industry for corrosion and wear resistant coating applications, and in emerging new areas such as electronics and biomedical industries, just to name a few. The basic premise in production of such coatings is the delivery of the coating material, originally in the form of a powder, through a high temperature gas jet (either a combusting flame jet or a plasma jet) onto a surface. Particles introduced into the jet stream heat up upon mixing with the hot jet gases and soften and/or melt before they impact at high velocities onto a surface to be coated. The microstructural characteristics of the coating depend strongly on the processing conditions of the powder; especially particle temperatures, velocities, and size distribution of the powder (Ref 1-6). These particle attributes affect the coating microstructure and bonding onto the substrate through the particle temperature and velocity at impact. For example, it has been shown that these particle parameters influence the types of splat formed upon particle impact (Ref 7, 8). Furthermore, different types of coatings have different optimum conditions for deposition. For example, high velocity, lower temperature conditions produced by high velocity oxygen fuel (HVOF) guns are appropriate for the delivery of metallic corrosion and wear resistant coatings. Conversely, ceramic-based coatings are typically produced by plasma jet systems, which produce conditions of high temperature and relatively low velocity compared to HVOF systems. It is, therefore, of interest to have both experimental and computational means of characterizing the particle velocity, size, and temperature fields in thermal spray delivery systems. This knowledge can be used in modeling of the particle deposition and coating formation processes.

Measurement of particle temperature, velocity, and size in high speed, chemically reacting, or ionized gas streams poses a significant challenge. Nonintrusive optical diagnostics must be relied on primarily, due to the hostile high temperature environment. The optical diagnostics need to be configured to minimize background influences and interference to obtain meaningful and accurate experimental data. Among the three particle measurements needed, particle velocity can be measured by laser Doppler velocimetry, which is based upon the Doppler shift of scattered light from a moving particle, a technique that is now a well-established method in fluid mechanics (Ref 9). In situ sizing of particles is typically based on the characteristics of light scattering, but it is a more difficult measurement. In the past decade, significant advances in the in situ sizing of smooth round particles were made by the technique of phase Doppler anemometry (Ref 10). Combining Doppler velocimetry and phase Doppler particle sizing technique has provided the ability

B.M. Cetegen and **W. Yu,** Mechanical Engineering Department, University of Connecticut, Storrs, CT 06269-3139. Contact B.M. Cetegen at e-mail: cetegen@engr.uconn.edu.

to simultaneously obtain both particle velocity and size in two-phase flows (Ref 11). Particle temperatures have been measured typically by multicolor radiation emission thermometry (Ref 3); a technique based upon the gray body thermal radiation emission by hot particles (Ref 12).

The preceding methods have been successfully implemented (Ref 2, 3, 13-15) on thermal spray (both HVOF and plasma) systems. While the combined radiation emission pyrometry and phase Doppler anemometry methods provide the most sophisticated and well-accepted research tools, its routine application on production facilities is not yet feasible due to the expertise needed for its successful application. Hence, other optical measurement systems have been developed to fill this need such as the DPV 2000 system developed by Moreau et al. (Ref 5).

The objective of this article is to provide new detailed experimental data on particle velocity, temperature, and size statistics obtained in a direct current (DC) arc plasma system using conventional and nanostructured, yttria-stabilized zirconia (YSZ) powders. These results are useful in (a) tailoring plasma spray conditions to achieve more durable and effective coating microstructure, (b) validating computational models of particle laden plasmas for their subsequent use in process optimization, and (c) determining the joint probability distributions of particle velocity, temperature, and size as inputs for the deposition and coating build-up models (Ref 16).

2. Experimental Procedure

2.1 Particle Velocity and Size Diagnostics

Particle velocity and size measurements were performed using an Aerometrics phase Doppler particle anemometer (PDPA). The PDPA system consists of the fiber optic light transmission unit, model No. XMT204-2.1 (Aerometrics, Sunnyvale, CA), coupled with an argon ion laser, model Innova 90-6 (Coherent, Santa Clara, CA), via a two-dimensional fiber drive, model No. FBD240-R (Aerometrics, Sunnyvale, CA). The laser light, which is scattered by the particles, is collected by the receiver unit, model No. RCV200-U (Aerometrics, Sunnyvale, CA). The transmitter and receiver are configured in the backscatter mode, as shown in Fig. 1. Signal processing is accomplished by Fourier transform-based real time processors at a maximum input frequency of 150 MHz. Processed data are stored in a laboratory computer for further analysis. Data acquisition system provides data validation checks on the raw data signals based on the Doppler burst features for velocity and the multiple phase measurements for particle diameter.

For the system configuration and the parameters employed, velocities in the range from –230 to 630 m/s and particle diameters between 0.5 and 150 μm were determined. In order to optimize the data validation rate both with respect to particle velocity and diameter, the system parameters (laser intensity, photomultiplier tube voltage, and sampling rate) were varied to obtain the highest data validation rate. While measurement validation with respect to velocity is typically greater than 90%, validation based on size criteria can be problematic, depending on the sphericity and surface smoothness of the particles passing through the probe volume. For the conventional YSZ powder used in these experiments, particles were quite spherical and smooth on their surface (see Fig. 2a) so that particle size validation rates between 25 and 75% were achieved. For the nanoclustered YSZ powder, particle surface roughness was higher, as shown in the micrograph of Fig. 2(b). Consequently, the size measurements with the PDPA instrument were difficult at best in the regions where melting and smoothing down of particle surface did not occur.

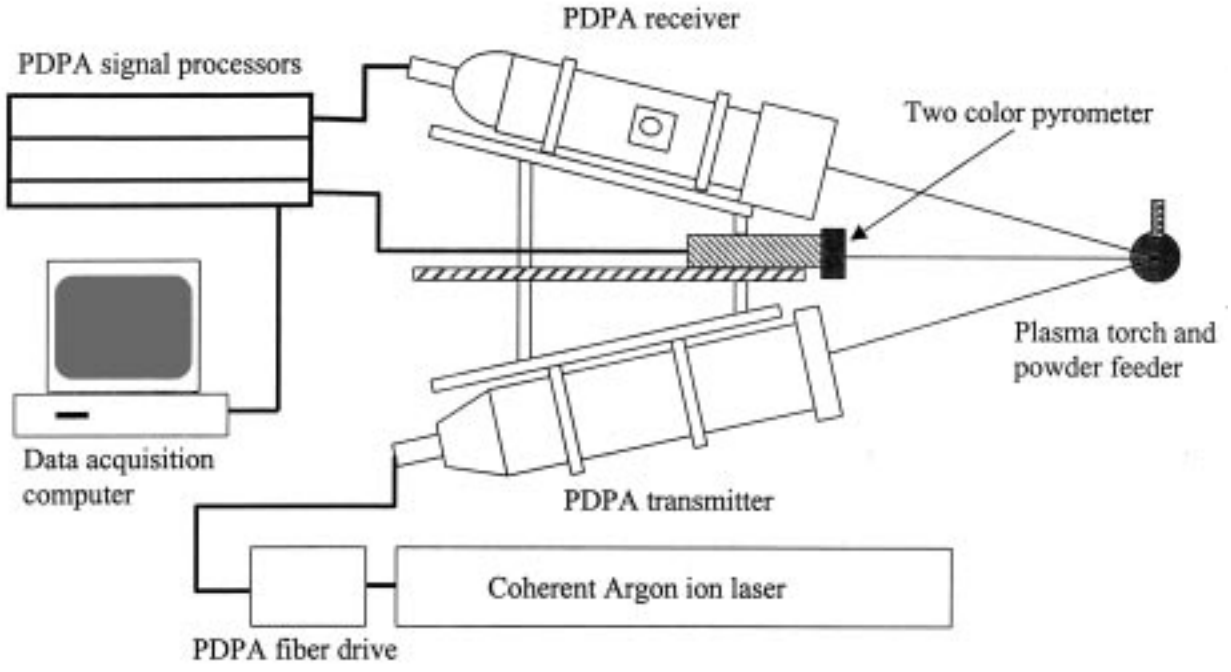

Fig. 1 Experimental configuration for the in-flight particle measurements

Another feature of the PDPA system is its capability of external input of other data streams when the PDPA system receives a validated data point. This feature was utilized to couple the PDPA measurements with the temperature measurements.

2.2 Particle Radiation Emission Thermometry

Particle temperature measurements were made using a custom built, two color pyrometer. The system consisted of a detector head containing an objective lens assembly, a bifurcated fiber optic, two bandpass filters, two photomultiplier detectors, voltage amplifiers, and a logarithmic circuit. The typical time constant for data acquisition was limited to 10 μs, as set by the frequency response of the electronic circuitry. The well-established principle of radiation thermometry is based upon the relationship of radiation intensity distribution to the emitting body temperature and wavelength through Planck's emission law (Ref 12) given by:

$$i_\lambda = \varepsilon_\lambda \frac{2C_1}{\lambda^5[\exp\ (C_2/\lambda T) - 1]} \qquad \text{(Eq 1)}$$

where, ε_λ is the spectral emissivity of the emitting surface, i_λ is the spectral radiation intensity, λ is the emission wavelength, T is the absolute temperature, and $C_1 = 0.5955 \times 10^8$ W · μm^4/(m^2 · steradian) and $C_2 = 1.4387 \times 10^4$ μm · K are the two Planck constants. When the intensities at two wavelengths λ_1 and λ_2 are measured, the emitter temperature can be found from:

$$\frac{1}{T} = \ln\left[\left(\frac{\lambda_1}{\lambda_2}\right)^5 \frac{\varepsilon_{\lambda_2} i_{\lambda_1}}{\varepsilon_{\lambda_1} i_{\lambda_2}}\right] / C_2\left(\frac{1}{\lambda_2} - \frac{1}{\lambda_1}\right) \qquad \text{(Eq 2)}$$

It is typically assumed that particle surface emissivities in the two nearby wavelength bands are the same (i.e., the gray body behavior between λ_1 and λ_2) so the temperature is a function of the intensity ratio:

$$T = C_2\left(\frac{1}{\lambda_2} - \frac{1}{\lambda_1}\right) / \ln\left[\left(\frac{\lambda_1}{\lambda_2}\right)^5 \frac{i_{\lambda_1}}{i_{\lambda_2}}\right] \qquad \text{(Eq 3)}$$

When this technique is applied in chemically reacting or plasma streams, it is important to avoid the strong spectral emission regions of the gas, which might interfere with the particle temperature measurement. Thus, a careful selection of the two color measurement wavelengths is necessary. Additionally, vaporization of the particle material components that exist as impurities such as sodium and other alkalines further complicates the measurement. For these reasons, emission spectra with and without the particles were first obtained in the Ar-H_2 plasma stream to determine the wavelength regions suitable for the temperature measurement. Figure 3 shows an example of these spectra. The two wavelength bands chosen were centered at 550 and 630 nm with 10 nm full width at half maximum (FWHM) bandwidths. The photocathode sensitivity of the photomultiplier tubes was also a factor in this selection. The system was calibrated using a blackbody oven over the temperature range (300 to 1300 K), while a tungsten strip lamp was used for higher temperatures (>1000 K). Figure 4 shows the calibration results for two optical configurations. The log-linear relationship implied in Eq 3 was obtained in these calibrations, which were then used to convert the output of the two color pyrometer to particle temperature.

2.3 Integration of PDPA and Two Color Temperature Instrumentation

The PDPA system was interfaced with the two color pyrometer as schematically shown in Fig. 1. The PDPA receiver and transmitter were mounted on a rigid frame in the backscatter mode at 150°. The two color pyrometer was configured

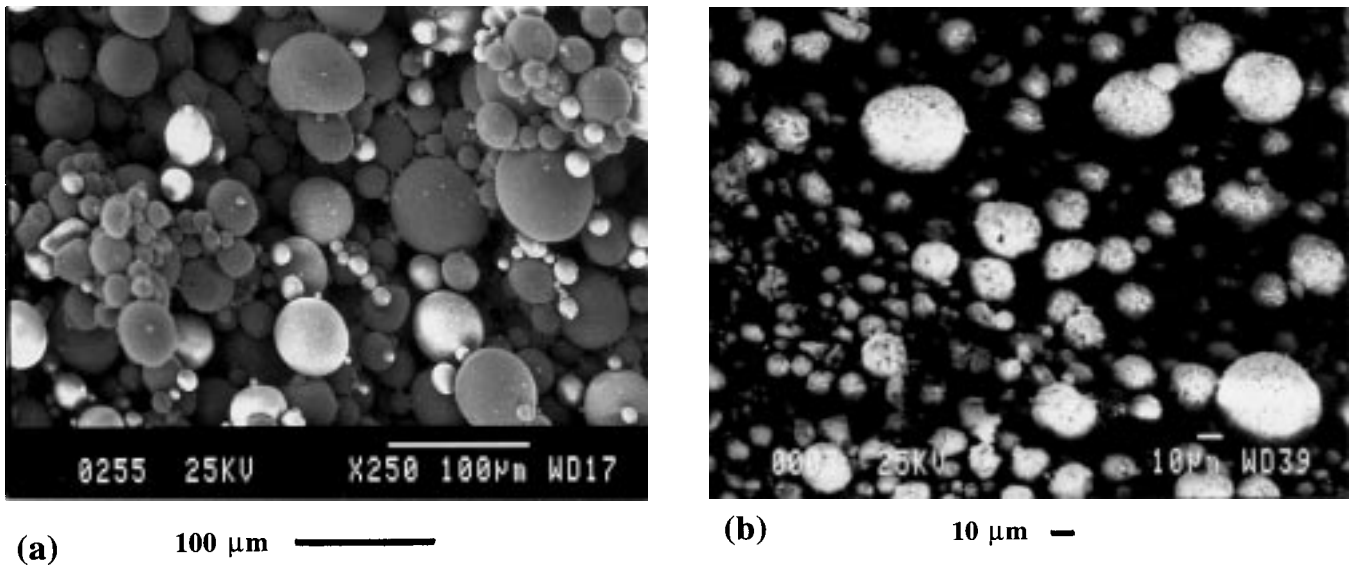

Fig. 2 Micrographs of the (a) conventional yttria-stabilized zirconia and the (b) nanoclustered yttria-stabilized zirconia used in the experiments. (Art has been reduced to 74% of its original size for printing.)

to observe the same focal region defined by the PDPA instrument. In this way, the same region of the flow field was interrogated by both measurement devices. The two color emission measurement of particle temperature represented a spatial average over a cylindrical particle-laden measurement volume of approximately 8 mm in diameter. Triggering of the temperature measurement upon detection of a particle by the PDPA instrument further discriminated the temperature measurement toward those particles detected by the PDPA instrument. This discrimination especially improved in dilute particle-laden flows where the low particle number density helped minimize the multiparticle effects. At each measurement location, 2000 to 3000 data samples were acquired to obtain statistically meaningful data. A larger number of measurements typically required long sampling periods with the attendant excessive use of powder.

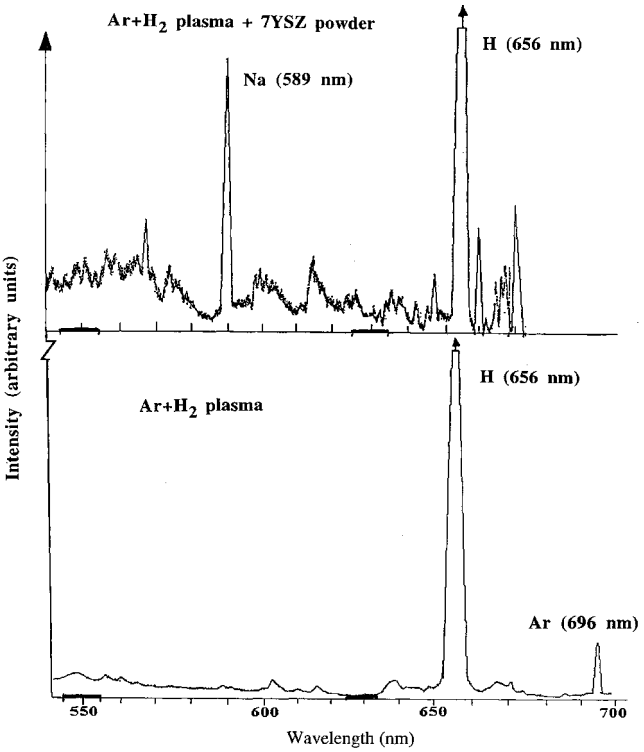

Fig. 3 Emission spectra of the argon-hydrogen plasma with and without yttria-stabilized zirconia powder

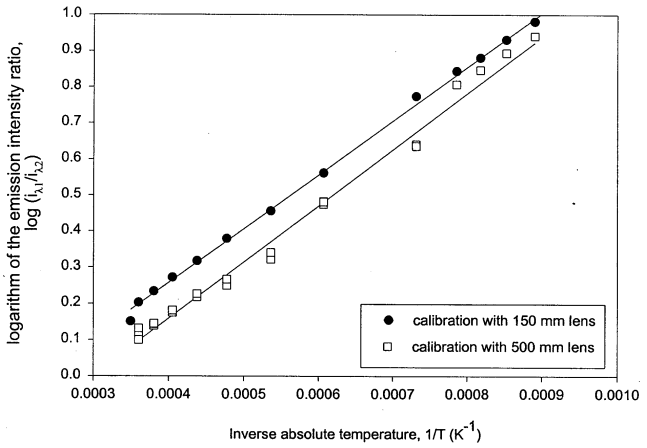

Fig. 4 Two color pyrometer calibrations

2.4 Experimental Conditions

The plasma system used was a direct current (DC) arc plasma unit, model No. 9MC, (Metco, Westbury, NY), equipped with Metco model No. 4MP particle feeder and model No. DJ3-3 plasma torch with transverse particle injection system. For the majority of the experiments reported here, a commercially available Metco (CE2279-2) 7.0 wt% yttria-stabilized zirconia (7YSZ) powder was used. The powder size distribution as received was 2.4% by weight for <25 μm, 12.1% for 25 to 38 μm, 27.5% for 39 to 75 μm, and 58.0% for 75 to 106 μm. The operating conditions for the plasma gun, equipped with the low speed Metco GH nozzle, were set at an arc current setting of 600 A, arc voltage of 60 V, argon flow rate of 2.27 m^3/h, and hydrogen flow rate of 0.59 m^3/h. The feed rate of the powder and the nitrogen carrier gas flow rates were 2.7 kg/h and 0.31 m^3/h, respectively. These values were selected for the optimum penetration of the powder stream into the plasma jet.

In a set of experiments with the conventional and nanoclustered 7YSZ powder, the high speed Metco GP nozzle was employed. The operating conditions for the plasma gun were arc current of 600 A, arc voltage of 60 V, and argon flowrate of 3.5 m^3/h. The powder and the nitrogen gas carrier flow rates were 2.7 kg/h and 0.42 m^3/h, respectively.

At each test condition, the axial and several radial distributions of particle axial velocity, diameter, and particle temperature, referred to as particle *V-d-T* hereafter, were obtained as schematically shown in Fig. 5. Some variations of the plasma parameters and the influence of the presence of a substrate on particle velocity were also investigated. Finally, injection of a nanostructured powder through the plasma jet was studied.

3. Results and Discussion

Characterization of the particle *V-d-T* distributions were carried out for the experimental conditions described earlier. In this section, the results are presented in the region of interest ($5 < Z < 10$ cm), typically employed in plasma thermal spray applications. Axial and several radial distributions of the measured quantities were obtained from 2000 to 3000 measurements at each measurement location. In the following paragraphs the averaged quantities as well as the distributions of the measured parameters are presented and discussed.

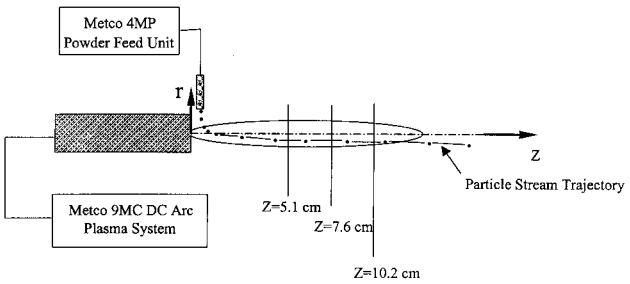

Fig. 5 Plasma measurement locations

3.1 Axial and Radial Distributions of V-d-T

Figure 6 shows the axial distributions of mean particle *V-d-T*. The mean particle velocity (Fig. 6a) increases in the early part of the plasma jet (at small *Z*) corresponding to the acceleration phase, followed by a decay farther downstream (at larger *Z*) due to entrainment of ambient air into the plasma jet and its consequent effect on particle velocity decay. The peak mean particle velocities were in the range of 150 to 155 m/s, which is typical for the employed operating conditions of the plasma thermal spray system. The particle size, as indicated here by the arithmetic mean particle diameter, D_{10}, decreased continuously with downstream distance along the plasma centerline. While this may first seem to be unrealistic, a closer look at the transverse injection scheme provides the explanation for this effect. As the particles of different sizes were injected through the transverse injection port, the larger particles penetrated further into the plasma jet, while the smaller particles were swept away by the high-speed plasma jet closer to the injection port. The result was an aerodynamic classification of particles with the larger particles populating more of the lower part of the plasma jet, which will be further discussed later in this paper. When averaged across the plasma jet at each axial location, the location averaged particle size shows this trend. Figure 6(b) shows the axial mean particle temperature variation in the plasma. The average particle temperatures are initially indicated to be above the zirconia melting point, suggesting some level of melting. With increasing downstream distance, particle temperatures fall below the melting point to temperature levels around 2500 to 2700 K. It should be mentioned however, that the uncertainty in the temperature measurement is approximately ±100 K. Hence, the location in the plasma, where equilibrium melting of particles may occur, can have uncertainties associated with the temperature measurement.

Figure 7 shows the radial distributions of *V-d-T* at three axial locations of $Z = 5.1$, 7.6, and 10.2 cm. In all these radial distributions, the particle velocity exhibits a skewed Gaussian distribution about the nozzle centerline with higher axial velocities occurring below the nozzle centerline at $r < 0$. This is believed to be due to the more effective acceleration of these particles that penetrate through the plasma jet. The radial classification of different size particles is also apparent in all three axial locations with the highest effect being closest to the injection site at $Z = 5.1$ cm (2.0 in.). With increasing downstream distance, high intensity turbulent mixing results in homogenization of the particle field.

Figure 7(d) shows the radial distributions of mean particle temperature at three downstream locations from the nozzle exit. It was found that the distributions were not symmetrical about the nozzle axis early on. The higher particle temperatures were observed below the plasma axis opposite the particle injection port. One explanation of this effect is that the particles that penetrated through the highest temperature plasma core region attained the higher temperatures. With increasing downstream distance, the radial distributions became flat, indicating homogenization of particle temperatures as a result of intense turbulent mixing. In general, the overall temperature levels decreased with increasing downstream distance.

One of the advantages of using this measurement system is the ability to acquire *V-d-T* data for a large number of samples at a given location and provide cross correlations among the measured parameters. Figure 8 shows the correlations between particle velocity—diameter and particle temperature—diameter at three radial positions at an axial location of $Z = 5.1$ cm. The three radial locations were chosen to represent the upper part, the center, and the lower part of the particle-laden plasma jet. The first observation is that the number of data realizations increased as the plasma jet traversed from the upper to the lower side across the injection port. The range of particle diameters present also increased toward the lower part of the jet. Consistent with the average particle diameter distributions, the small particles were swept into the upper part of the jet near the particle injection port. At the lower part of the plasma jet, larger size particles that penetrated through the core of the jet were responsible for the larger size range. The particle velocities were also somewhat higher at and below the plasma centerline as these particles gained higher velocities, having been accelerated in the high velocity regions of the plasma jet. However, there appears to be no strong correlation between the particle size and velocity at a given location.

The particle temperatures were in the range of 2600 to 3600 K at $r = 6.0$ mm location, indicating that some of the particles were unmelted. Because PDPA size data validation is sensitive to particle surface smoothness, the higher data rates were

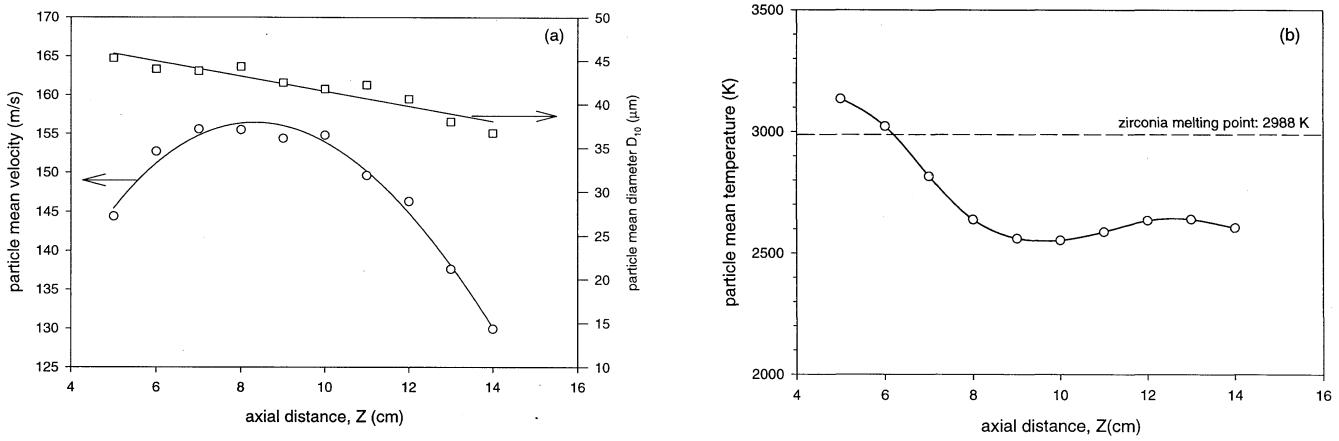

Fig. 6 Axial distributions of the mean particle velocity in the axial direction, mean particle size, and temperature

obtained in those regions where some degree of surface melting occurred. The improvement of the data rate at the $r = 0.0$ and –6.0 locations is believed to be a result of this effect. Indeed, particle temperatures were higher at these two radial locations with almost all particles having some level of melting at $r = –6.0$ mm. Because melting causes particles to become smooth, their size measurements by the PDPA instrument have a higher data validation rate. This may provide an indirect measure of the degree of particle melting. Figure 9 shows the radial profiles of the PDPA size validation rate at the three axial positions. It was found that the highest validation rates were observed below the plasma axis (i.e., $r<0$), where particles that penetrated through the plasma core were present.

3.2 Particle Velocity and Size Histograms

Figures 10 and 11 show the distributions of the particle velocity and size at several different locations in the plasma jet. In Fig. 10, the particle diameter histograms at three radial locations ($r = –8.0$, 0.0, and 10.0 mm) and two axial locations of $Z = 5.1$ and 10.2 cm are shown. Particle diameter histograms indicate an increasing population of larger particle sizes as the plasma jet is traversed toward the opposite side of the injection port (i.e., from top to bottom) at $Z = 5.1$ cm. For example, the population of 40 to 60 μm size range is significantly enhanced at $r = –8.0$ mm. The size distributions are consistent with the size distribution of the powder feed material. With increasing downstream distance at $Z = 10.2$ cm, the particle size distribution at the upper edge of the plasma jet remains similar to that at $Z = 5.1$ cm, populated mostly with particles less than 40 μm in size. At $Z = 10.2$ cm, the size distributions at $r = 0.0$ and –8.0 mm locations appear to be similar to those at $Z = 5.1$ cm. The reduction in the mean diameter at $r = –8.0$ mm and $Z = 10.2$ cm is attributed to turbulent entrainment of small particles into this region with increasing downstream distance.

The velocity histograms, shown in Fig. 11, exhibit broad or double peak distributions near the upper edge of the plasma jet, whereas the center and lower parts have normal distributions. The main reason for the existence of low velocity particles near the upper edge is the presence of small particles that track the flow well and become entrained into the mixing zones of the plasma jet with the stagnant ambient air. These regions have consequently lower axial velocities. It is interesting also to note that this effect was much less pronounced in the lower part of the plasma jet where the larger particles with more ballistic characteristics exhibited higher axial velocities. While the mean velocities were slightly lower at the lower edges than the center part of the plasma jet, the distributions remained fairly similar. The mean axial velocities increased with increasing downstream distance as found at $Z = 10.2$ cm.

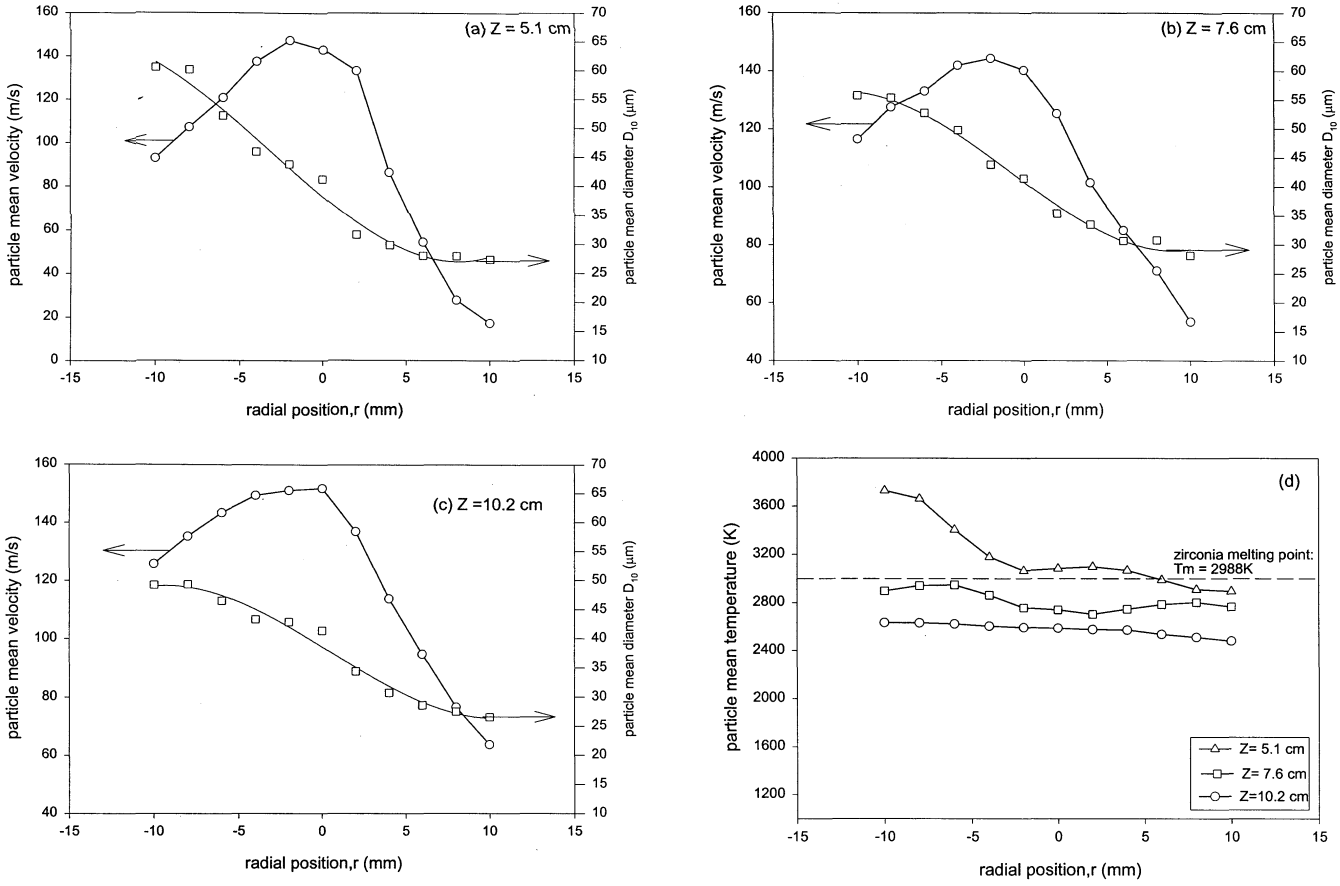

Fig. 7 Radial distributions of the mean particle velocity in the axial direction, mean particle size at three axial locations. (a) $Z = 5.1$ cm. (b) $Z = 7.6$ cm. (c) $Z = 10.2$ cm. (d) Radial distribution of the mean particle temperatures at the same three axial locations

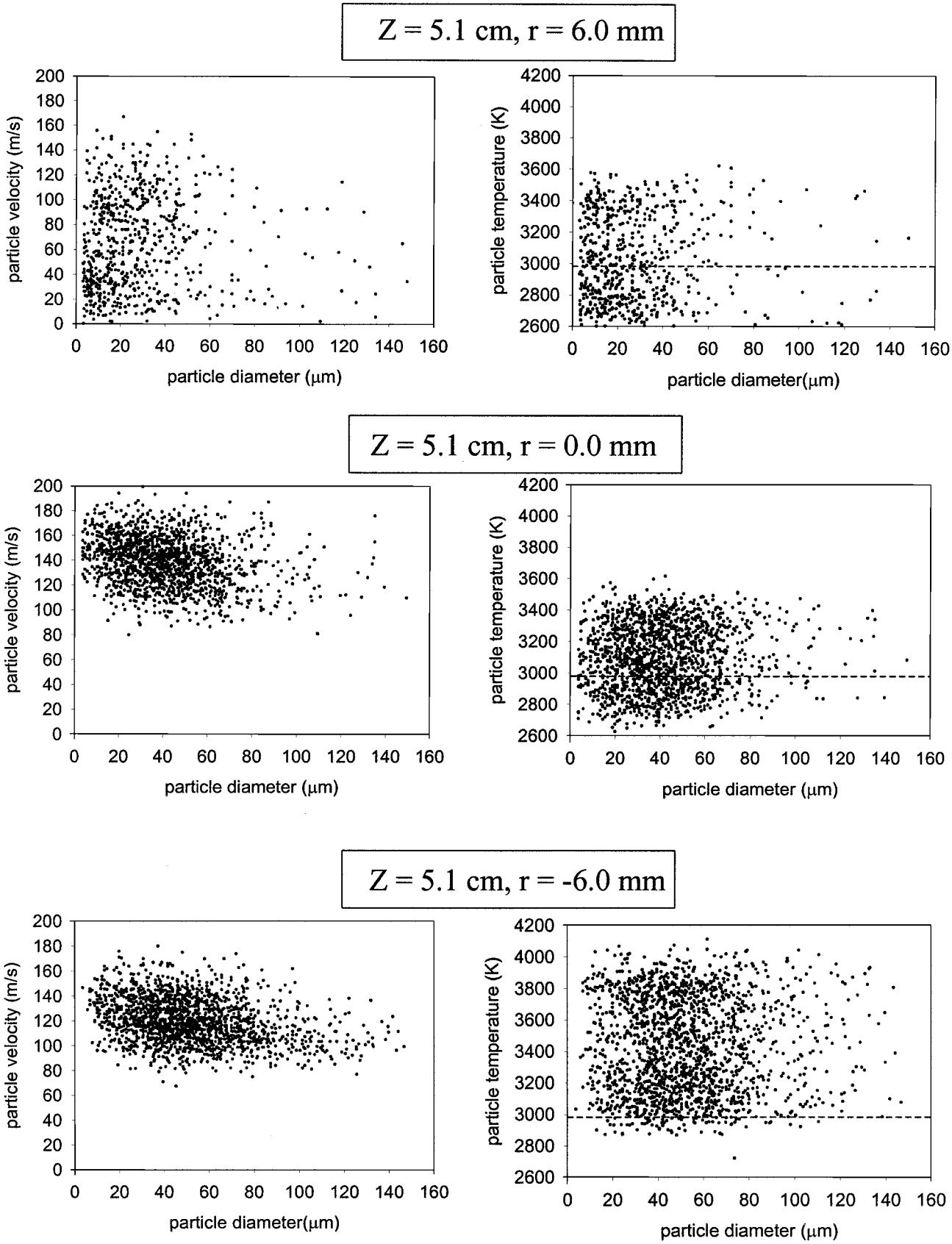

Fig. 8 Scatter plots of particle-diameter velocity (left column) and particle-diameter temperature (right column) at an axial location of $Z = 5.1$ cm at three selected radial locations. Zirconia melting temperature is shown as horizontal dotted lines.

3.3 Influence of Plasma Operating Parameters

Influence of plasma arc current and the argon flow rate were investigated in this study as well. Figure 12 shows these effects at a location of Z = 7.6 cm. The mean particle velocity increased with increasing arc current, particularly for those particles that traversed across the plasma jet (i.e., particles at $r < 0$). There appeared to be little or no effect on the velocity of the smaller particles in the upper part of the jet. Particle size distributions did not appear to be influenced by the plasma power variation, suggesting that appreciable particle fragmentation does not occur upon heat up. Figure 12(b) shows the influence of argon flow rate when it was varied by a factor of two. The mean particle velocities were found to increase with increasing argon flow rate, especially in the region across the injection port. A two-fold increase in argon flow rate resulted in a maximum velocity change of 38%. This reduced effect is attributed to the decay of velocity in the jet due to turbulent mixing and entrainment. The particle size distribution was unaffected by the argon flow rate as expected.

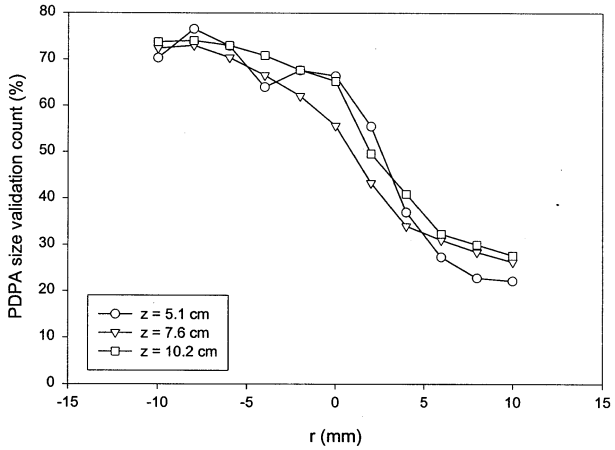

Fig. 9 Distribution of the data validation rate based on the size measurement at three axial locations

3.4 Effect of a Substrate on Particle Velocity

The presence of a substrate stagnating the plasma jet flow was also investigated in this study. Because thermal spray coatings

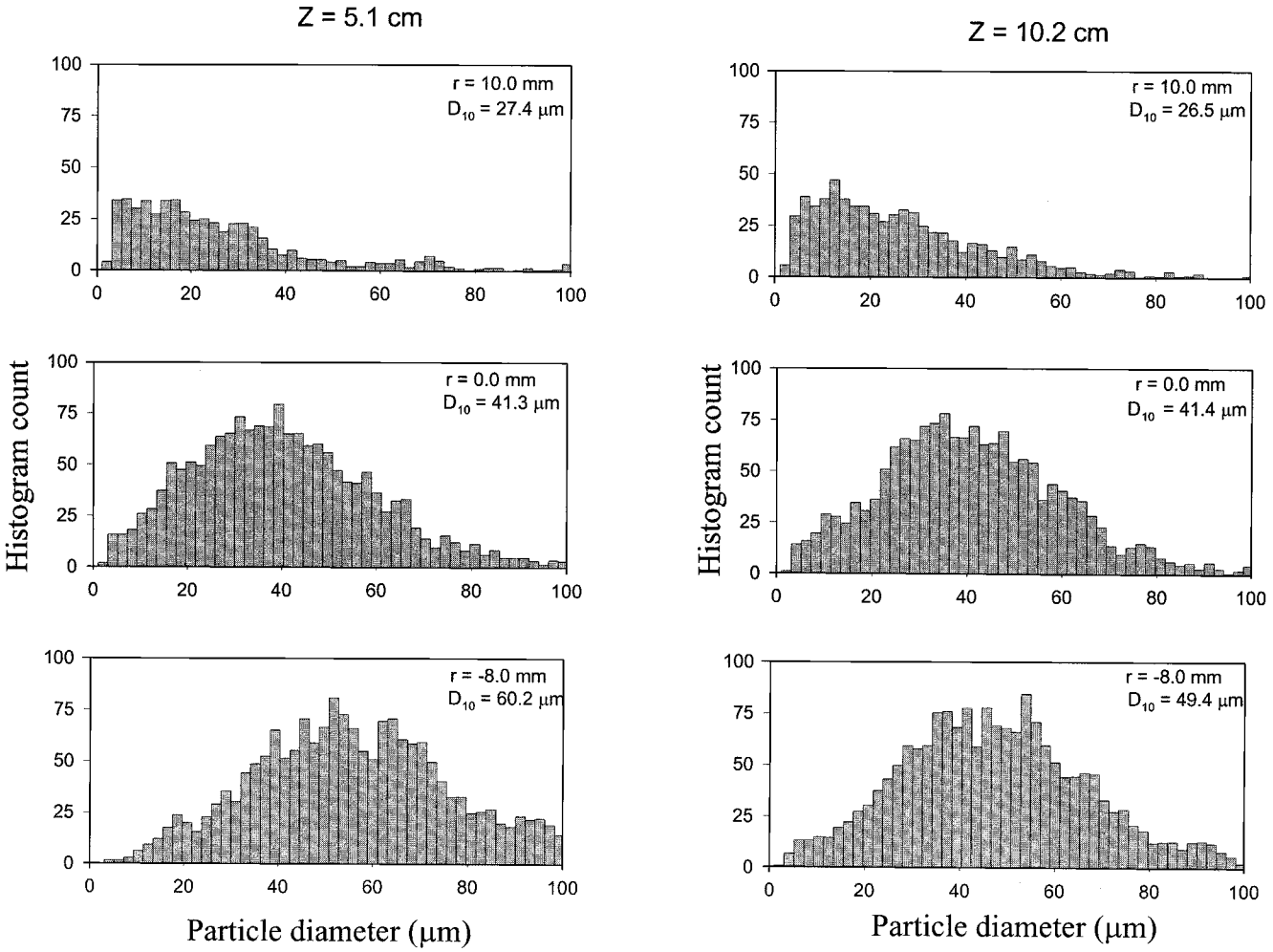

Fig. 10 Particle size histograms in the plasma jet at selected locations. Left column at Z = 5.1 cm and r = + 10.0 mm, 0 mm, and –8.0 mm. Right column at Z = 10.2 cm and r = +10.0 mm, 0 mm, and –8.0 mm.

were applied onto a substrate in this configuration, it is useful to know whether particles slowed down toward the stagnation region. Figure 13 shows the radial distribution of mean particle velocity at an axial location of $Z = 7.6$ cm with and without a substrate located 5 mm downstream of the measurement location. It was found that the substrate had a minimal effect of less than 5% reduction of the particle velocity. This result suggests that particle motion is essentially ballistic, and slowing of particles due to flow divergence near the stagnation region does not significantly influence the particle velocity.

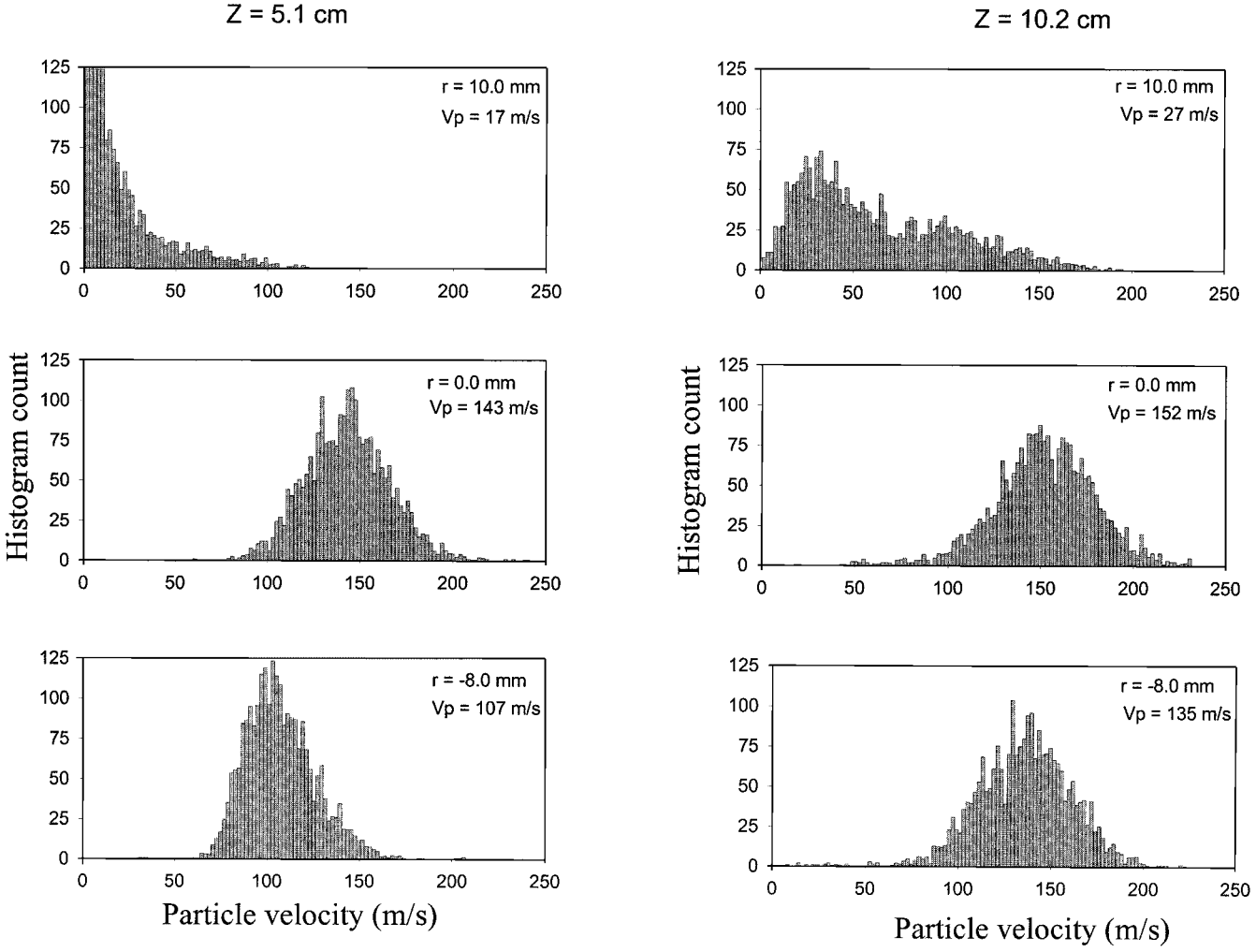

Fig. 11 Particle axial velocity histograms in the plasma jet at selected locations. Left column at $Z = 5.1$ cm and $r = +0.0$ mm, 0 mm, and –8.0 mm. Right column at $Z = 10.2$ cm and $r = +10.0$ mm, 0 mm, and –8.0 mm.

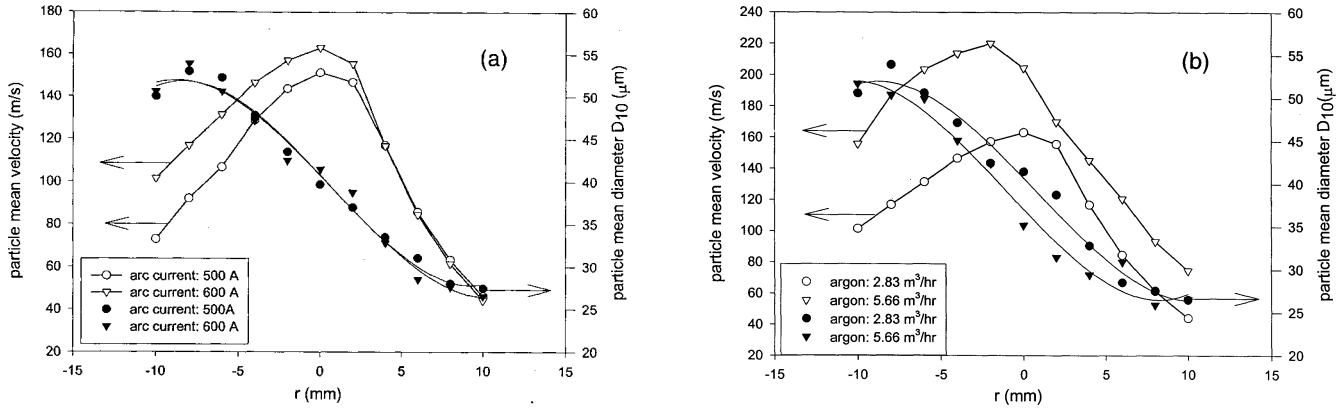

Fig. 12 Radial distributions of the mean particle velocity (axial) and particle size as influenced by the plasma current (a) and argon flow rate (b)

3.5 *Plasma Spraying of Nanoclustered YSZ Powder*

With the contemporary interest in producing nanostructured coatings, recent experiments have focused on injection of nanoclustered YSZ through a plasma jet. The nanoclusters contained many small (of the order of 10 to 50 nm) grains that were bound together to form relatively spherical particles of <30 μm mean diameter (Ref 17) as shown in the micrograph of Fig. 2(b).

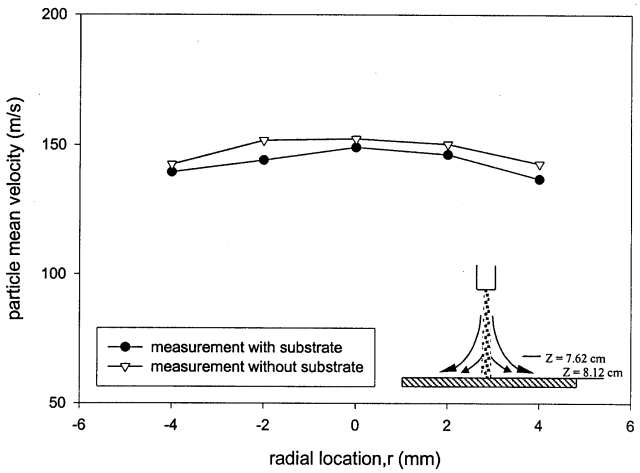

Fig. 13 Impact of the presence of a substrate on axial particle velocity

Due to the limited availability of this powder, only a few experiments were performed to characterize the particle *V-d-T* at an axial location of *Z* = 7.6 cm. Because of the desired processing conditions, a high-speed plasma nozzle (Metco GP) was used for thermal spraying. Both the conventional and the nanopowders were injected into the plasma jet under identical injection conditions. In Fig. 14, the particle velocity, size, temperatures, and PDPA data rates were compared for the conventional 7YSZ powder and the 7YSZ nanopowder. It was found that the peak particle velocities were somewhat higher for the nanoclustered powder in comparison to those for the conventional powder. It also appears that the maximum velocity location shifted below the plasma gun axis.

The particle size measurements were difficult at best with the nanopowder due to the large surface roughness of the nanoclusters (Fig. 2b). The data validation rate was very low at most measurement locations. Thus, the particle mean diameter variation, shown in Fig. 14(b), has a high degree of uncertainty due to the low-size validation rate. Figure 14(c) shows the radial temperature profiles at *Z* = 7.6 cm. The mean particle temperatures were found to be 150 to 200 K lower than the conventional

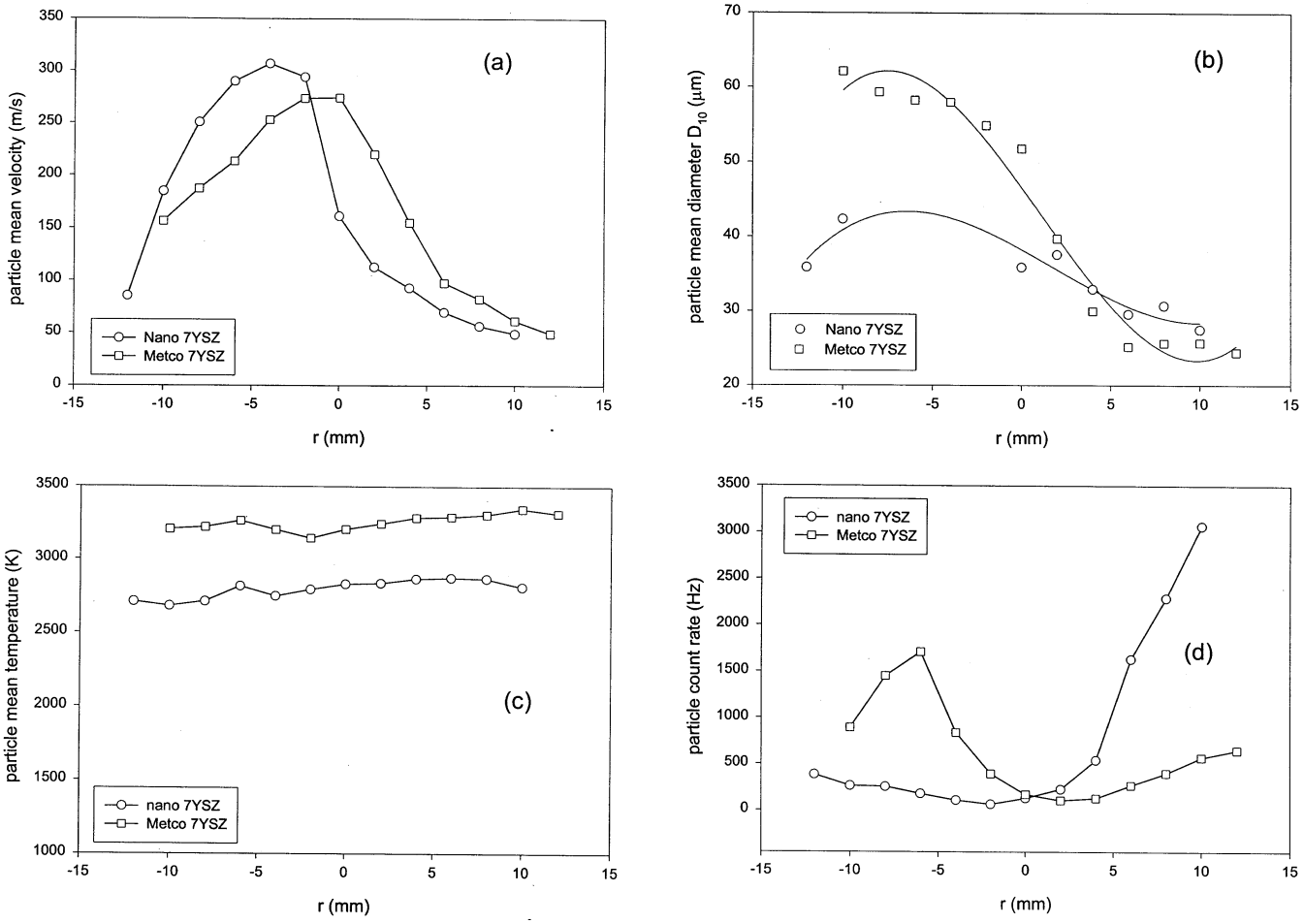

Fig. 14 Comparison of the (a) mean particle velocity, (b) size, (c) temperature, and (d) particle count rate for the conventional and the nanostructured yttria-stabilized zirconia powder at an axial location of *Z* = 7.6 cm

powder particles. It is speculated that the nanoclusters, which were typically in a hollow shell form, were less capable of penetrating through the higher temperature zones of the plasma and, therefore, were not heated to as high temperatures as the conventional powder. This can be seen in the particle count rate comparison shown in Fig. 14(d), which suggests that the particle count rates are low in the regions below the plasma axis where the particles that penetrated through the plasma would have been. Most of the particles were swept above the plasma axis, thus bypassing the high temperature core region of the plasma.

4. Conclusions

Experimental results on temperature, velocity, and size measurements in DC arc plasma thermal sprays are reported in this article. Experiments were performed using a conventional DC arc argon-hydrogen plasma with two different 7 wt% YSZ powders injected transversely into the plasma jet. Measurements were performed along the centerline of the plasma jet as well as radial profiles at several axial positions. From typical data samples consisting of 2000 to 3000 measurements at each location, distributions and average values of the measured parameters are reported. It was found that the transverse injection of the powder results in aerodynamic size classification of the powder in the jet with the large particles penetrating further across the plasma jet than the smaller particles, which were more readily swept by the high momentum of the plasma jet. Average particle temperatures showed a good degree of uniformity radially and decayed in magnitude with increasing downstream distance. There is good indication that the particles that penetrated through the plasma jet attained surface temperatures above the melting point of zirconia. Smaller particles were typically swept by the high plasma jet momentum and did not reach the high temperatures. Implications of these effects could be significant in terms of coating quality because the deposition of melted large particles and unmelted small particles will influence the coating microstructure. Furthermore, the spatial nonuniformities were expected to further accentuate these effects. Based on these findings, axial injection of powder into plasma jets may overcome some of the nonuniformities in the particle properties (size and temperature) typically associated with the transverse injection scheme. Experiments to assess the effects of the presence of a downstream stagnation plate, as it exists in thermal spray applications, showed only a small effect on axial particle velocities, confirming that the particles moved under ballistic conditions after their initial acceleration. Injection of nanoclustered particles was also studied. Significant differences in particle velocities and temperatures were observed for the nanoclustered powder in comparison to the conventional powder under the same plasma operating and particle injection conditions. This points to the need for optimization of the injection of nanostructured powders in thermal spray processes.

Acknowledgments

The research reported herein was sponsored by the Office of Naval Research under grant No. N00014-97-0843 under the direction of Dr. Lawrence Kabakoff. The instrumentation used in this research was acquired through Army Research Office Grant No. 37312-MS-RIP. The authors are thankful to Dr. Danny Xiao, Mr. Christopher Strock, and Mr. Meidong Wang of Inframat Corporation for their assistance in the operation of the thermal spray facility.

References

1. L. Pawlowski, *The Science and Engineering of Thermal Spray Coatings*, Wiley, 1995
2. R.N. Wright, J.R. Fincke, W.D. Swank, and D.C. Haggard, Particle Velocity and Temperature Influences on the Microstructure of Plasma Sprayed Nickel, *Thermal Spray: Practical Solutions for Engineering Problems*, C.C. Berndt, Ed., ASM International, 1996, p 511
3. J.R. Fincke, W.D. Swank, and D.C. Haggard, A Particle Temperature Sensor for Monitoring and Control of the Thermal Spray Process, *Thermal Spray Science and Technology*, C.C. Berndt and S. Sampath, Ed., ASM International, 1995, p 774
4. M. Prystay, P. Gougeon, and C. Moreau, Correlation between Particle Temperature and Velocity and Structure of Plasma Sprayed Zirconia Coatings, *Thermal Spray: Practical Solutions for Engineering Problems*, C.C. Berndt, Ed., ASM International, 1996, p 992
5. C. Moreau, P. Gougeon, M. Lamontagne, V. Lacasse, G. Vaudreuil, and P. Cielo, On-Line Control of the Plasma Spraying Process by Monitoring the Temperature, Velocity and Trajectory of In-Flight Particles, *Thermal Spray Industrial Applications*, C.C. Berndt and S. Sampath, Ed., ASM International, 1994, p 431
6. M. Vardelle, A. Vardelle, P. Fauchais, and M.I. Boulos, Particle Dynamics and Heat Transfer under Plasma Conditions, *AIChE J.*, Vol 34 (No. 4), 1988, p 567-573
7. A.C. Leger, M. Vardelle, A. Vardelle, P. Fauchais, S. Sampath, C.C. Berndt, and H. Herman, Plasma Sprayed Zirconia: Relationships Between Particle Parameters, Splat Formation and Deposit Generation-Part I: Impact and Solidification, *Thermal Spray: Practical Solutions for Engineering Problems*, C.C. Berndt, Ed., ASM International, 1996, p 623
8. G. Montavon, C.C. Berndt, C. Coddet, S. Sampath, and H. Herman, Quality Control of the Intrinsic Deposition Efficiency from The Controls of the Splat Morphologies and the Deposit Microstructure, *J. Therm. Spray Technol.*, Vol 6 (No. 2), 1997, p 153-166
9. F. Durst, A. Melling, and J.H. Whitelaw, *Principles and Practice of Laser-Doppler Anemometry*, 2nd ed., Academic Press, 1981
10. W.D. Bachalo, M.J. Houser, Phase/Doppler Spray Analyzer for Simultaneous Measurements of Droplet Size and Velocity Distributions, *Opt. Eng.*, Vol 23, 1983, p 583-590
11. M.S. Tageldin and B.M. Cetegen, Development of Mixing and Dispersion in an Isothermal, Droplet-Laden, Confined Turbulent Mixing Layer, *Combust. Sci. Tech.*, Vol 130, 1997, p 131-169
12. M. Planck, The Theory of Heat Radiation, Dover, 1959
13. J.R. Fincke, S.B. Jeffrey, and S.B. Englert, In-Flight Measurement of Particle Size and Temperature, *J. Phys. E: Sci. Instrum.*, Vol 21, 1988, p 367-370
14. J.R. Fincke, W.D. Swank, and C.L. Jeffery, Simultaneous Measurements of Particle Size, Velocity and Temperature in Thermal Plasmas, *IEEE Trans. Plasma Sci.*, Vol 18 (No. 6), 1990
15. M.F. Smith, T.J. O'Hern, J.E. Brockmann, R.A. Neiser, and T.J. Roemer, A Comparison of Two Laser-Based Diagnostics for Analysis of Particles in Thermal Spray Streams, *Thermal Spray Science and Technology*, C.C. Berndt and S. Sampath, Ed., ASM International, 1995
16. I. Ahmed, T.L. Bergman, and B.M. Cetegen, A Thermal Model of the Spray Deposition of Ceramic Particles onto a Metallic Surface, Internal Report, Mechanical Engineering Dept., University of Connecticut, June 1998
17. B.H. Keer and P.R. Strutt, Nanostructures: The Next Generation of High Performance Bulk Materials and Coatings, *Naval Research Reviews*, Vol XLVI (No. 4), 1994, p 4